

High-Throughput Design of Peierls and Charge Density Wave Phases in Q1D Organometallic Materials

Prakriti Kayastha¹ and Raghunathan Ramakrishnan^{1*}

¹Tata Institute of Fundamental Research, Centre for Interdisciplinary Sciences, Hyderabad 500107, India

(Dated: January 26, 2021)

Soft-phonon modes of an undistorted phase encode a material's preference for symmetry lowering. However, the evidence is sparse for the relationship between an unstable phonon wavevector's reciprocal and the number of formula units in the stable distorted phase. This “ $1/q^*$ -criterion” holds great potential for the first-principles design of materials, especially in low-dimension. We validate the approach on the Q1D organometallic materials space containing 1199 ring-metal units and identify candidates that are stable in undistorted (1 unit), Peierls (2 units), charge density wave (3-5 units), or long wave (> 5 units) phases. We highlight materials exhibiting gap-opening as well as an uncommon gap-closing Peierls transition, and discuss an example case stabilized as a charge density wave insulator. We present the data generated for this study through an interactive publicly accessible Big Data analytics platform (<https://moldis.tifrh.res.in/data/rmq1d>) facilitating limitless and seamless data-mining explorations.

Materials stabilized in low-dimension offer maximum tunability of properties through external perturbations—an understanding of their dynamical behavior is crucial for rational materials design[1]. The soft-phonon mode in an undistorted phase steers geometric distortions culminating in modulated superstructures. The corresponding change in the electron density gives rise to a charge density wave (CDW)[2]. Peierls transition is a unique case of CDW where the maximally unstable phonon wavevector (q) in a Q1D material is at the edge of the first Brillouin zone, X[3]. Studies on synthesis and characterization of quasi-one-dimensional (Q1D) organic/organometallic materials are abound in anticipation of observing exceptional CDW properties. CDW materials exhibit a broad range of anisotropic electric, thermal or interesting dynamical behaviour[4–10]. Some widely characterized Q1D conductors exhibiting CDW stabilization are mixed-valence planar transition metal complexes and transition metal chalcogenides[11–13], while prominent Q1D insulators are of the ABX_3 -type showing anisotropic magnetism[14–16]. Low-dimensional materials such as carbon nanotubes, nanoribbons[17–19] and conjugated polymers[20, 21] show high thermoelectric performance in their Peierls phase.

In this study, we present a strategy for the rational design of dynamically stable phases of Q1D materials using information encoded in the phonon band structure of the undistorted, translationally symmetric phase. Our approach builds on the fact that the number of units preferred in low symmetric phase corresponds to maximal instability at $q^* = 1/N$; for integer N , we find a commensurately modulated phase. Although generally every $N > 1$ indicates a CDW, in this study, we refer to the $N = 2$ case as Peierls. While Peierls stabilization is associated

with a metal-to-insulator transition, some studies have reported a reduction in translational symmetry through

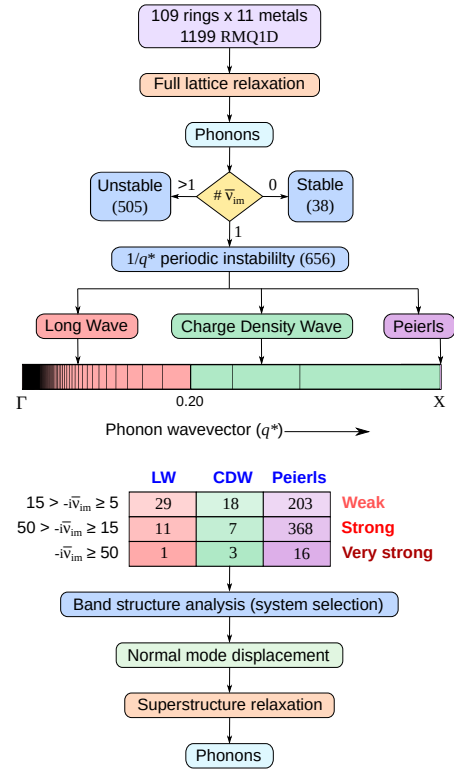


FIG. 1. Workflow for high-throughput modeling of RMQ1D materials: Characterization of dynamic stability is based on the number of imaginary phonon modes (\bar{v}_{im} is the wavenumber) and maximally unstable phonon wavevector (q^*). Discrete spectrum points to commensurate values of q^* . Integer-valued $1/q^*$ gives the number of units in Peierls, Charge Density Wave or Long Wave superstructure phases. Numbers reported can be generated on-the-fly by data-mining at (<https://moldis.tifrh.res.in/data/rmq1d>); see Supplementary Information (SI) for query screenshots.

* ramakrishnan@tifrh.res.in

transverse displacements without gap-opening at the zone-edge[22, 23]. The $1/q^*$ criterion generalizes Peierls and Jahn-Teller-type instabilities—both effects marked by the distortion of a symmetric structure. The former is signified by a gap opening at the band’s zone-edge, while the latter is accompanied by the lifting of degeneracy in the highest occupied molecular orbital—amounting to opening a gap in molecular orbitals. Irrespective of the final outcome, i.e., gap-opening at the level of bands or orbitals, the overall structural instability is characteristic of the dynamic stability of a geometry on the material potential energy surface. Hence, the presence of dynamic instability in a system constitutes a necessary condition for superstructure formation, whereas the presence of a metallic band in the undistorted phase, a sufficient one.

To validate our high-throughput strategy based on the $q^* = 1/N$ criterion for designing translationally low symmetric phases, we select 1D chain of alternate ring-metal units (RMQ1D)[24]. The materials space is composed of 11 monovalent metals (Na–Cs, Cu–Au, Al–Tl) bonded to any of the 109 rings generated by substituting C atoms in a cyclopentadienyl anion (Cp) with all possible valencies of B, N, and S. Cp complexes with Li^+ and Na^+ , form an eclipsed chain, while K^+ , In^+ and Tl^+ prefer a zigzag form[25, 26]. The structures are stable because they minimize repulsion due to ring-ring interactions as well as interactions between the ring and the distorted core of the metal[27, 28]. Formation of such structures has escaped inspection in the light of Peierls instability because of the lack of gap-opening in these materials that remain as insulators before and after distortion. On the other hand, the longitudinal distortion in $\text{B}_2\text{C}_3\text{H}_5\text{Ni}$ leads to widening of the Ni bands that is inextricably coupled with the dimerization of the units[29, 30]. Such Q1D materials are unknown for the d^{10} metals, and for combinatorially varying heteroatom-substituted Cp. For comprehensive coverage and data-driven analysis, we present an *ab initio* high-throughput workflow (Figure 1). Such an automated strategy has gained popularity for the design of molecular[31–34] and materials[35–37] Big Data.

Based on the nature of phonon instability, our high-throughput workflow characterizes stationary points on the material potential energy surface into three classes: (i) stable with positive phonons, (ii) those with maximum instability in a (degenerate or non-degenerate) normal mode, and (iii) unstable with imaginary frequencies in several modes. Distribution of the 1199 materials into these classes and further analysis of the stability was performed through data-mining, see Figure 1. With a threshold of 5 cm^{-1} for the imaginary wavenumbers’ norms, we find 38 materials belonging to class-i, stabilizing in the 1U phase with one ring-metal formula unit. In class-ii, we find 656 materials that provide a scope to apply the $1/q^*$ criterion for stabilizing in a Peierls, CDW, or long wave phase through normal mode displacements followed by superstructure relaxation. While our flow characterized

505 RMQ1Ds as unstable (class-iii), with multiple imaginary phonon modes, one cannot rule out the possibility of locating a local minimum on the potential energy surface for these stoichiometries when starting with a unit cell arrangement with lateral packing.

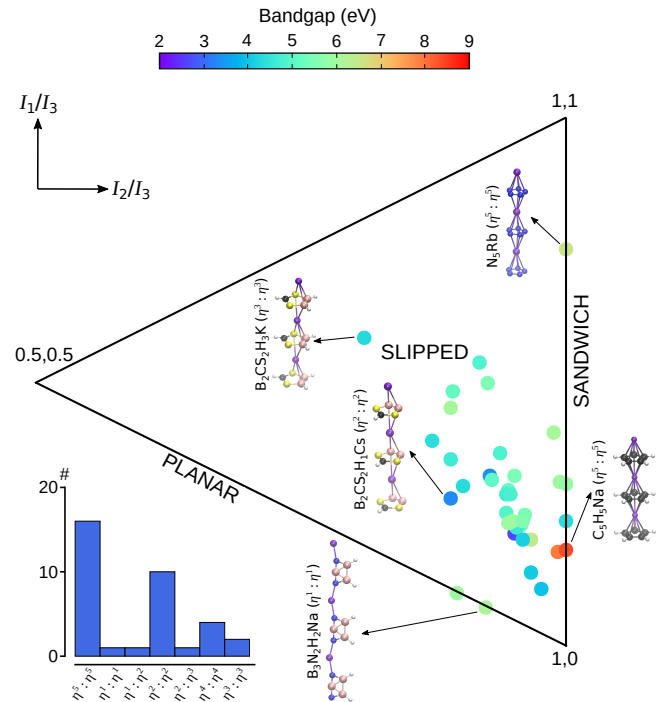


FIG. 2. Shape distribution of RMQ1D materials stable in the 1U phase, with one formula unit. The axes correspond to normalized principal moments of inertia I_1/I_3 and I_2/I_3 , respectively, with $I_1 \leq I_2 \leq I_3$. For 38 dynamically stable materials, PBE0 band gaps are color-coded. The inset shows the distribution of their hapticities (η).

We identify 38 dynamically stable 1U materials with large band gaps, $\epsilon_g \geq 2\text{ eV}$. Three of these, including CpNa characterized by diffraction[25], exhibit positive phonon wavenumbers throughout the Brillouin zone, while for the rest 35, we observed imaginary wavenumbers of small magnitudes ($< 5\text{ cm}^{-1}$). The computed value for the longitudinal lattice constant of CpNa is 4.74 \AA , which is within $< 1\%$ error compared to the experimental value 4.71 \AA . The most distinguishing feature of the systems stable in the 1U phase is that they are exclusively alkali metal-based. Figure 2 provides a bird’s-eye view of the structural diversity and band gaps of the 38 1U systems. Materials showing ring-opening or fragmentation have been eliminated; these rings exhibit strong σ -donation to the metal center resulting in a loss of bonding electrons needed to stabilize the ring framework.

Along the $I_1/I_3 = 1 - I_2/I_3$ line in the shape distribution plot, one finds purely planar structures formed by metal ions σ -bonded to the rings. On the $I_2/I_3 = 1$ vertical line, one finds eclipsed $\eta^5 : \eta^5$ sandwich structures with Cp and N_5 rings. The top-most point

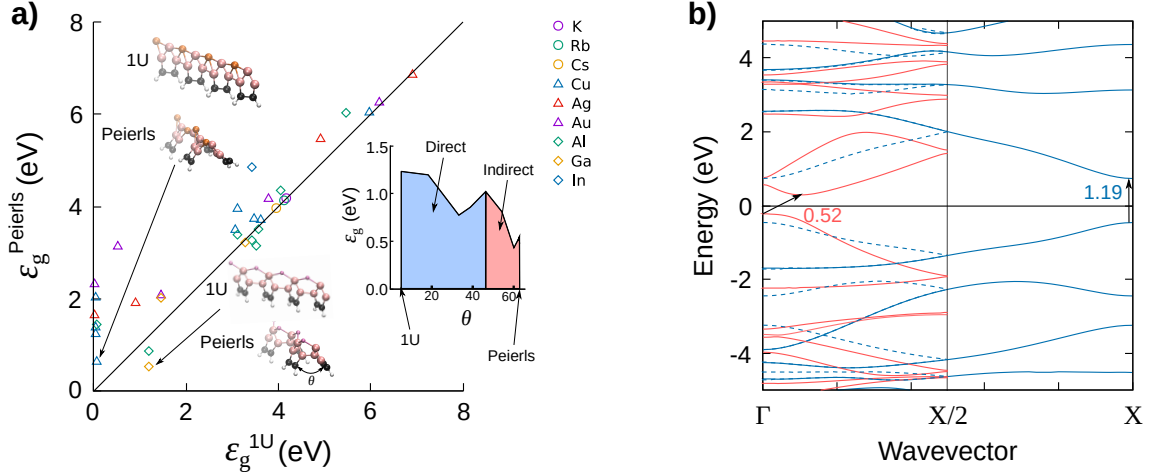


FIG. 3. Influence of Peierls stabilization on electronic band gap, ε_g for 33 selected Peierls materials: a) Comparison of ε_g , of 1U and Peierls phases. Structures of gap-opening (with Cu) and gap-closing (with Ga) cases containing the $B_3C_2H_2$ ring are shown. Variation in ε_g of $B_3C_2H_2Ga$ during 1U-to-Peierls geometry relaxation is shown in the subplot. b) Band folding and gap-closing in $B_3C_2H_2Ga$. Band structures of 1U (blue solid lines), 2U superstructure (blue dashed lines) and Peierls (red solid lines) phases are shown. Arrows point to band gaps and Fermi energy level is set to 0 eV.

corresponds to the most elongated sandwich complex N_5Rb ; while $CpNa$, at the bottom, is the most compact. In the latter, the lattice constant is more than twice the ring-metal distance; indicating weak crystal packing leading to high-volatility similar to the experimentally studied $CpGa$ [26]. These trends are in line with the ionic radii of the corresponding metals.

Structures with $\eta^2/\eta^3/\eta^4$ -bonding arise predominantly for hetero-substituted rings with cations slipped away from the geometric center of the ring. Experimentally, $CpNa$ has been identified as a 1U system with an $\eta^5 : \eta^5$ pattern[25], which is confirmed by our calculations (see Figure 2). However, the same metal in combination with substituted Cp rings shows a diverse coordination pattern due to lowering of the ring symmetry. Out of 1199 RMQ1D materials, thermodynamically most and least stable are $B_2NS_2H_2Cs$ (formation energy, $E_f = -0.877$ eV), and B_3CNHCu ($E_f = 1.290$ eV), respectively; neither are dynamically stable in the 1U phase. The pentazole ring, N_5^- , isolable in an acidic medium[38] prefers equatorial σ -bonding with cations[39]. Our results indicate hard acid ions like Cs^+ or Rb^+ to form N_5^- complexes through $\eta^5 : \eta^5$ coordination pattern. However, the same ring when complexed with the soft acid ions Cu^+ , Ag^+ and Au^+ forms $\eta^1 : \eta^1$ σ -bonding. Thermodynamic stability of these materials correlates poorly with their dynamic stability, made apparent by the fact that E_f of the 38 materials stabilizing in the 1U phase uniformly span a window of -0.726 to 0.992 eV.

RMQ1D materials that are neither unstable nor stable in the 1U phase comprise potential cases for Peierls (587), CDW (28), and long wave (41) transitions. Peierls materials are detected by a phonon instability at $q^* = X$ (see Figure 1). Given that the experimental

evidence for RMQ1D materials stabilized by a Peierls transition are far and few between, it is of interest to characterize those preferring a low symmetric phase in our modeling. Presently it is not computationally feasible to perform refined investigations of all 587 Peierls candidates. Hence, we select the most important subsets including 16 materials with $|\bar{\nu}_{im}| \geq 50$ cm^{-1} expected to show a large gain in the potential energy via soft-mode distortions. Besides, we choose 10 Peierls candidates containing the rings Cp , $B_3C_2H_2^-$, or N_5^- ; the latter two have been selected to understand the impact of σ -aromaticity on the geometry. We also include 7 gap-opening Peierls candidates that are metallic in the 1U phase. Starting from the 2U superstructure of the 1U geometries and a subsequent distortion along the soft-mode of the 1U phase, a full geometry relaxation was performed for these 33 materials.

Irrespective of the bandgap modulation, all 33 Peierls materials undergo structural distortions deviating from the 1U structure, augmented by a net drop in the total energy. A comparison of ε_g in the Peierls and dynamically unstable 1U phases reveals some interesting trends (Figure 3a). The magnitude of ε_g in the Peierls phase varies inversely with that of the 1U phase. Materials with a large gap in the 1U phase ($\varepsilon_g > 3$ eV) show a small gain in the bandgap going to the Peierls phase. A common structural characteristic in all the gap-opening Peierls candidates is a slippage of the metal ions—especially Al, Cu, Ag, and Au—away from the ring center resulting in poor shielding of the metallic bonds by the rings in the 1U phase. Figure S1 in the SI presents the relaxed structures of all 33 Peierls cases. Overall, 7 of these exhibit strong gap-opening and 3 prefer an uncommon gap-closing Peierls transition, $\varepsilon_g^{Peierls} < \varepsilon_g^{1U}$. It is well-known that at finite-temperature, the

Peierls structural distortion is lifted[20]. In RMQ1D materials, such a transition may be observed for the 33 Peierls cases. Thermalization of the electronic states[40] may be achieved with a large Fermi temperature for a frozen geometry. However, a more satisfactory dynamic picture may be obtained only through atomistic modeling revealing a thermalized, symmetric lattice structure as experimentally noted for perovskites[41].

Of all selected Peierls materials, most show a gap-opening transition (Figure 3a). As an example of a material undergoing a gap-closing transition, the structure of $B_3C_2H_2Ga$ is shown in the inset of Figure 3a. Compared to the bands in the 1U phase, those in the Peierls phase are shifted down (Figure 3b). However, the doubly degenerate levels of the folded 1U bands at $E = 2$ eV lie far above E_F to remove this degeneracy. An indirect bandgap in the Peierls phase is due to the energy ordering of bands and their alignments. The dip in the lowest conduction band is due to an avoided crossing between the bands immediately below and above E_F showing mixed characteristics near the Γ -point. We verified this fact through an orbital analysis. Dependence of the band mixing on distortion along the angle θ is illustrated in the inset to Figure 3a. For the 1U phase, θ is 4.43° . Since the character of the unstable phonon mode in the 1U phase is essentially angular, Peierls distortion brings negligible change in the metal-metal distance, going from 3.76 Å to 3.69 Å. During geometry relaxation of the 1U phase's 2U structure, θ converges to 62.64° at the Peierls phase. The characteristic of the bandgap changes from direct to indirect at $\theta \approx 45^\circ$.

Following an analysis of the 1U phonon spectrum of the 23 CDW candidates, we select cases for which the magnitude of the maximally unstable phonon mode is $\geq 50 \text{ cm}^{-1}$ and the corresponding wavevector coinciding with the commensurate values: $q^* = 1/3$, $q^* = 1/4$ and $q^* = 1/5$, shown as a stick spectrum in Figure 1. Further analysis revealed only 4 out of 23 to show commensurate phonon instability. Electron density of the 1U material is a periodic repetition of its unit cell density, ρ^u :

$$\rho^{1U}(z) = \rho^u \cos(2Xz). \quad (1)$$

In the commensurately modulated phase, the 1U density is distorted by a periodic superstructure wave of amplitude $\Delta\rho^s$ and wavelength $1/q^*$

$$\rho^{NU}(z) = \rho^{1U}(z) + \Delta\rho^s \cos(zq^*). \quad (2)$$

The only potential CDW material satisfying our selection criteria is B_3NSH_3Cu whose unit cell details and phonon band structures are on display in Figure 4. In the 1U phase, the metal centers are separated by 3.51 Å with the ring shielding the interaction between adjacent metal centers rendering the material an insulator, $\varepsilon_g^{1U} = 1.16 \text{ eV}$. While the 1U phonon band structure shows prominent instability at $q = 2X/3$, one also notes another band exhibiting instability at $X/3$, albeit with phonon wavenumber of a smaller magnitude. In the 1U phase,

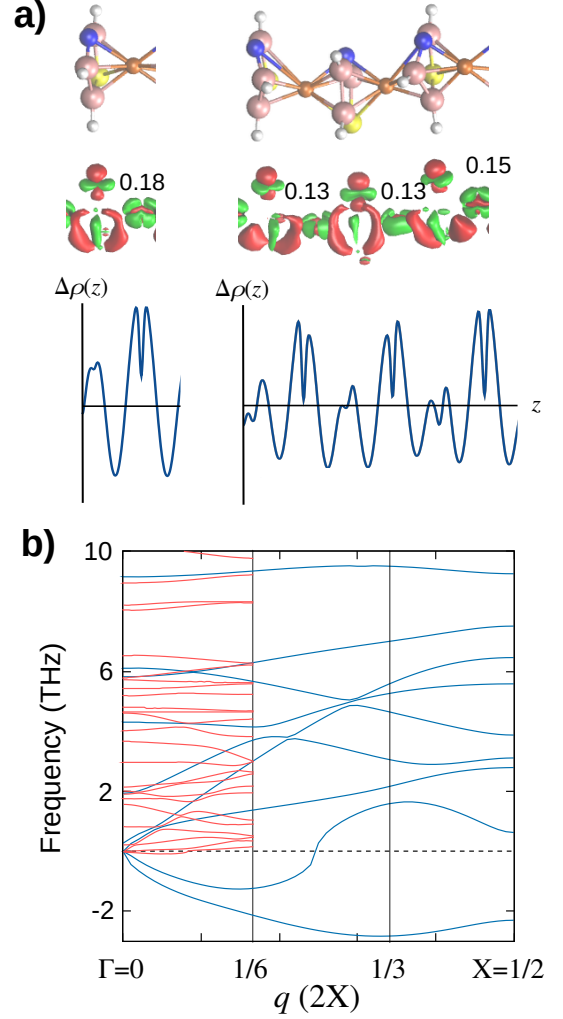


FIG. 4. Charge density wave formation in B_3NSH_3Cu : a) Unit cell arrangements in 1U (left) and CDW (right) phases are shown along with the density difference, $\Delta\rho(\mathbf{r})$, calculated by subtracting the densities of rings and metals from the solid. Green and red denote gain and depletion of electron density, respectively. Mulliken charges on the Cu centers are stated in units of e . Also shown is the longitudinal density difference, $\Delta\rho(z)$ (blue solid line). b) Phonon band structures of the 1U (blue lines) and the CDW (red lines) phases; the zone-edge X is π/c , where c is the lattice constant.

a partial electron transfer from the anionic ring to the metal center is indicated by the net Mulliken charge on Cu, $q_{Cu}^M = 0.18e$. The density difference $\Delta\rho(\mathbf{r}) = \rho(\mathbf{r}) - \rho_{rings}(\mathbf{r}) - \rho_{metals}(\mathbf{r})$ illustrates regions of electron density gain and depletion upon ring-metal bonding in the solid. Better clarity is attained with the reduced density difference, by integrating $\Delta\rho(\mathbf{r})$ in the plane perpendicular to the lattice vector resulting in the 1D fingerprint, $\Delta\rho(z) = -\int \int dxdy \Delta\rho(\mathbf{r})$. The shape and periodicity of $\Delta\rho(z)$ coincide with the structural and charge density variations of the material.

Full geometry relaxation based on the soft-mode distortion of the 3U superstructure was done as

previously stated for the Peierls cases. Transitioning to the dynamically stable CDW phase, the material trimerizes with a net drop in the E_f by 0.031 eV. Overall, the material shows further widening of the electronic gap to 1.97 eV, the corresponding phonon spectrum confirms a dynamically stable phase (Figure 4b). The visible effect in the structure is a repeated chain of two distinct units: a metal-ring-metal trimer, with 2 equivalent Cu atoms ($q_{\text{Cu}}^{\text{M}} = 0.13e$) which is displaced from a ring-metal-ring fragment along a transverse direction. Based on this arrangement, one can interpret the structure of $\text{B}_3\text{NSH}_3\text{Cu}$ through a ‘pseudo’-Peierls transition of the 3U superstructure phase. This structural description agrees with the periodic variation of $\Delta\rho(\mathbf{r})$ and q_{Cu}^{M} , while the reduced density fingerprint conveys further information that are not perceptible from the other quantities. Within the metal-ring-metal fragment, one notes $\Delta\rho(z)$ coinciding with Cu to split in an asymmetric fashion. This is an indication of a weak bonding between the Cu atoms of metal-ring-metal, leaving the single Cu-center ($q_{\text{Cu}}^{\text{M}} = 0.15e$) of ring-metal-ring in an environment similar to that of the 1U phase. While the amplitude of $\Delta\rho(z)$ is uniform across the lattice for the 1U phase, it is undulatory for the CDW phase.

To conclude, we identify stable phases of RMQ1D materials based on maximum instability in the phonon spectrum of the translationally symmetric phase with one unit. Among those with multiple unstable phonon modes, there are potential candidates that may be stabilized by a weak lateral packing in the bulk phase. While our high-throughput workflow also identifies long wave candidates potentially distorting to a periodic structure containing > 5 Us, it is beyond the scope of the present study to embark on their characterization. However, it may be anticipated that the polymer design strategy based on a soft-phonon will be less reliable for the long wave cases because of the residual uncertainties associated with the methods used in resolving $q^* < 0.2$. The procedures applied here can be extended to materials comprising open-shell metal ions to identify candidates stabilized by magnetic moments, or half-metals relevant for spin-conduction[42]. However, a high-throughput study of magnetic RMQ1D will incur severe computational complexities because of the challenges associated with the determination of the ground state among competing spin-states. For heavier atoms, besides, spin-orbit coupling needs to be incorporated for realistic modeling. Extending the ideas presented here to higher-dimensional phases requires the phonon wavevector to have more components. For instance, distortion of the square-net phase of H atoms (1U phase) in 2D to a tetrameric phase (4 Us in the unit cell)[43] is indicated by maximal phonon instability, $\mathbf{q}^* = (0.5, 0.5)$ in the 1U phase. The catalog of materials presented here can be further extended by considering other rings, metals, and their hetero-combinations. The results presented here and further explorations of them through the publicly accessible interactive data-mining

framework, may leverage rational experimental design of Q1D materials with tunable electronic properties.

COMPUTATIONAL DETAILS

Geometry optimizations of the anion rings were performed using the program package Gaussian16[44] with the PBE0[45] density functional theory method and a def2-TZVP basis set. After eliminating unconverged, non-planar and acyclic structures, the resulting 109 rings were combined with monovalent cations to construct unit cell geometries for periodic calculations. An initial lattice constant of minimum $c = 5.0$ Å—with the metal placed at $c/2$ Å from the ring—and \mathbf{a} and \mathbf{b} vectors of length 50 Å were used to emulate vacuum. Full relaxation of RMQ1Ds were performed with the all-electron, numeric atom-centered orbital code FHI-aims[46] with the PBE[47] functional. In all calculations, we used $1 \times 1 \times 64$ k -grids, and tight, tier-1 basis set for all atoms. Lattice vectors and atomic coordinates were fully relaxed with electron density converged to $10^{-6} e/\text{\AA}^3$, analytic forces to 5×10^{-4} eV/Å, and the maximum force component for lattice relaxation to 5×10^{-3} eV/Å. Phonon spectra were obtained with a 113 supercell using finite-derivatives of analytic forces with an atomic displacement of 0.005 Å and tighter thresholds ($10^{-7} e/\text{\AA}^3$ for density; 10^{-6} eV/Å for analytic forces) using Phonopy[48] interfaced with FHI-aims. These control settings yield converged results as shown in Table S2 and Table S3 in the SI. Table S1 compares the performance of the PBE functional with other semilocal and hybrid ones. Since the packing interaction in the RMQ1D materials is essentially ionic in nature, van der Waals correction to PBE influences the geometries and phonons negligibly. The lack of critical long-range interactions in the RMQ1D materials is also indicated by the fact that the PBE results are comparable to that of the hybrid methods HSE03 or PBE0. Treatments at the latter level are necessary for accurate modeling of Peierls phases with significant long-range interaction within the unit cell as noted for polyacetylenes[49]. Single point calculations were performed with the PBE0 functional for accurate estimations of total energies and band gaps.

SUPPLEMENTARY MATERIAL

The supplementary material contains: (i) additional tables with results benchmarking the performance of DFT methods and control parameters for selected RMQ1D materials, (ii) reference chemical potential for calculating formation energies, and (iii) screenshots for data-mining (see Data Availability).

ACKNOWLEDGMENTS

RR gratefully acknowledges Prof. Matthias Scheffler for providing a license to the FHI-AIMS program. The authors thank Salini Senthil for setting up the data-mining framework. We acknowledge support of the Department of Atomic Energy, Government of India, under Project Identification No. RTI 4007. All calculations have been performed using the Helios computer cluster, which is an integral part

of the MolDis Big Data facility, TIFR Hyderabad (<https://moldis.tifrh.res.in>).

DATA AVAILABILITY

The data that support the findings of this study are openly available at (<https://moldis.tifrh.res.in/data/rmq1d>). Input and output files of corresponding calculations are deposited in the NOMAD repository (<https://nomad-lab.eu/>).

-
- [1] M. Cao, X. Wang, M. Zhang, J. Shu, W. Cao, H. Yang, X. Fang, and J. Yuan, *Adv. Funct. Mater.* **29**, 1807398 (2019).
 - [2] G. Grüner, *Rev. Mod. Phys.* **60**, 1129 (1988).
 - [3] R. E. Peierls, *Quantum Theory of Solids* (Clarendon Press, 1996).
 - [4] A. Casian, *Phys. Rev. B* **81**, 155415 (2010).
 - [5] X.-S. Ye, Y.-J. Liu, X.-H. Zeng, and G. Wu, *Sci. Rep.* **5**, 17358 (2015).
 - [6] G. A. Toombs, *Phys. Rep.* **40**, 181 (1978).
 - [7] S. Etemad and A. Heeger, *Annu. Rev. Phys. Chem.* **33**, 443 (1982).
 - [8] A. J. Heeger, S. Kivelson, J. Schrieffer, and W.-P. Su, *Rev. Mod. Phys.* **60**, 781 (1988).
 - [9] T. Giamarchi, *Chem. Rev.* **104**, 5037 (2004).
 - [10] J. Ahn, J. Byun, H. Koh, E. Rotenberg, S. Kevan, and H. Yeom, *Phys. Rev. Lett.* **93**, 106401 (2004).
 - [11] J. Gopalakrishnan and K. Nanjundaswamy, *Bull. Mater. Sci.* **5**, 287 (1983).
 - [12] R. Hoffmann, S. Shaik, J. Scott, M.-H. Whangbo, and M. J. Foshee, *J. Solid State Chem.* **34**, 263 (1980).
 - [13] J.-K. Bao, J.-Y. Liu, C.-W. Ma, Z.-H. Meng, Z.-T. Tang, Y.-L. Sun, H.-F. Zhai, H. Jiang, H. Bai, C.-M. Feng, *et al.*, *Phys. Rev. X* **5**, 011013 (2015).
 - [14] J. Ackerman, E. Holt, and S. Holt, *J. Solid State Chem.* **9**, 279 (1974).
 - [15] A. Harrison, M. Collins, J. Abu-Dayyeh, and C. Stager, *Phys. Rev. B* **43**, 679 (1991).
 - [16] Y. Endoh, G. Shirane, R. Birgeneau, P. M. Richards, and S. Holt, *Phys. Rev. Lett.* **32**, 170 (1974).
 - [17] S. Piscanec, M. Lazzeri, J. Robertson, A. C. Ferrari, and F. Mauri, *Phys. Rev. B* **75**, 035427 (2007).
 - [18] D. Connétable, G.-M. Rignanese, J.-C. Charlier, and X. Blase, *Phys. Rev. Lett.* **94**, 015503 (2005).
 - [19] V. Tozzini and V. Pellegrini, *Phys. Rev. B* **81**, 113404 (2010).
 - [20] X. he, S. Ryu, and S. Hirata, *J. Chem. Phys.* **140**, 024702 (2014).
 - [21] L. M. Tolbert and X. Zhao, *J. Am. Chem. Soc.* **119**, 3253 (1997).
 - [22] I. P. Batra, *Phys. Rev. B* **42**, 9162 (1990).
 - [23] I. P. Batra, *Surf. Sci.* **242**, 354 (1991).
 - [24] M. C. Böhm, *One-dimensional Organometallic Materials: An Analysis of Electronic Structure Effects*, Vol. 45 (Springer Verlag, 1987).
 - [25] R. E. Dinnebier, U. Behrens, and F. Olbrich, *Organometallics* **16**, 3855 (1997).
 - [26] A. J. Downs, *Chemistry of Aluminium, Gallium, Indium and Thallium* (Springer Science & Business Media, 1993).
 - [27] E. Canadell, O. Eisenstein, and J. Rubio, *Organometallics* **3**, 759 (1984).
 - [28] I. Bytheway, P. L. Popelier, and R. J. Gillespie, *Can. J. Chem.* **74**, 1059 (1996).
 - [29] W. Siebert, *Pure Appl. Chem* **60**, 1345 (1988).
 - [30] M. Y. Lavrentiev, H. Köppel, and M. C. Böhm, *Chem. Phys.* **169**, 85 (1993).
 - [31] J. Hachmann, R. Olivares-Amaya, S. Atahan-Evrenk, C. Amador-Bedolla, R. S. Sánchez-Carrera, A. Gold-Parker, L. Vogt, A. M. Brockway, and A. Aspuru-Guzik, *J. Phys. Chem. Lett.* **2**, 2241 (2011).
 - [32] R. Ramakrishnan, P. O. Dral, M. Rupp, and O. A. von Lilienfeld, *Sci. Data* **1**, 140022 (2014).
 - [33] S. Chakraborty, P. Kayastha, and R. Ramakrishnan, *J. Chem. Phys.* **150**, 114106 (2019).
 - [34] S. Senthil, S. Chakraborty, and R. Ramakrishnan, *arXiv preprint arXiv:2010.02635* (2020).
 - [35] S. Curtarolo, G. L. Hart, M. B. Nardelli, N. Mingo, S. Sanvito, and O. Levy, *Nat. Mater.* **12**, 191 (2013).
 - [36] A. Jain, S. P. Ong, G. Hautier, W. Chen, W. D. Richards, S. Dacek, S. Cholia, D. Gunter, D. Skinner, G. Ceder, *et al.*, *APL Mater.* **1**, 011002 (2013).
 - [37] S. Kirklin, J. E. Saal, B. Meredig, A. Thompson, J. W. Doak, M. Aykol, S. Rühl, and C. Wolverton, *Npj Comput. Mater.* **1**, 1 (2015).
 - [38] L. Zhang, C. Yao, Y. Yu, S.-L. Jiang, C. Q. Sun, and J. Chen, *J. Phys. Chem. Lett.* **10**, 2378 (2019).
 - [39] K. O. Christe, *Science* **355**, 351 (2017).
 - [40] V. V. Deshpande, M. Bockrath, L. I. Glazman, and A. Yacoby, *Nature* **464**, 209 (2010).
 - [41] M. S. Kirschner, B. T. Diroll, P. Guo, S. M. Harvey, W. Helweg, N. C. Flanders, A. Brumberg, N. E. Watkins, A. A. Leonard, A. M. Evans, *et al.*, *Nat. Commun.* **10**, 1 (2019).
 - [42] L. Wang, Z. Cai, J. Wang, J. Lu, G. Luo, L. Lai, J. Zhou, R. Qin, Z. Gao, D. Yu, *et al.*, *Nano Lett.* **8**, 3640 (2008).
 - [43] R. Hoffman, *Solids and Surfaces: A Chemist's View of Bonding in Extended Structures* (Wiley-VCH, 1989).
 - [44] M. J. Frisch *et al.*, "Gaussian16 Revision C.01," (2016), Gaussian Inc. Wallingford CT 2016.
 - [45] C. Adamo and V. Barone, *J. Chem. Phys.* **110**, 6158 (1999).
 - [46] V. Blum, R. Gehrke, F. Hanke, P. Havu, V. Havu, X. Ren, K. Reuter, and M. Scheffler, *Comput. Phys. Comm.* **180**, 2175 (2009).

- [47] J. P. Perdew, K. Burke, and M. Ernzerhof, Phys. Rev. Lett. **77**, 3865 (1996).
- [48] A. Togo and I. Tanaka, Scr. Mater **108**, 1 (2015).
- [49] G. Dumont, P. Boulanger, M. Côté, and M. Ernzerhof, Phys. Rev. B **82**, 035419 (2010).